frontiers | Frontiers in Physics

TYPE Original Research
PUBLISHED 28 May 2024
DOI 10.3389/fphy.2024.1404504

OPEN ACCESS

EDITED BY
Quan Sheng,
Tianjin University, China

REVIEWED BY
Giuseppe Brunetti,
Politecnico di Bari, Italy
Kai Zhong,
Tianjin University, China

*CORRESPONDENCE
N. N. Yudin,
rach3@yandex.ru

†These authors have contributed equally to this work and share first authorship

RECEIVED 21 March 2024
ACCEPTED 10 May 2024
PUBLISHED 28 May 2024

CITATION
Yudin NN, Zinoviev MM, Podzyvalov SN, Kuznetsov VS, Slyunko ES, Lysenko AB, Kalsin AY, Gabdrakhmanov AS, Yakovlev SV, Sadovnikov SA, Romanovskii OA and Baalbaki H (2024), Tunable optical parametric oscillator based on $ZnGeP_2$ crystal for greenhouse gas remote sensing systems.
Front. Phys. 12:1404504.
doi: 10.3389/fphy.2024.1404504

Tunable optical parametric oscillator based on $ZnGeP_2$ crystal for greenhouse gas remote sensing systems

N. N. Yudin[1,2*†], M. M. Zinoviev[1,2†], S. N. Podzyvalov[1†], V. S. Kuznetsov[1†], E. S. Slyunko[1†], A. B. Lysenko[1†], A. Yu. Kalsin[1†], A. Sh. Gabdrakhmanov[1†], S. V. Yakovlev[2†], S. A. Sadovnikov[2†], O. A. Romanovskii[2†] and H. Baalbaki[1†]

[1]Scientific Educational Center "Optical and Photonic Technologies", National Research Tomsk State University, Tomsk, Russia, [2]Institute of Atmospheric Optics SB RAS, Tomsk, Russia

This work is devoted to the development of a compact source of coherent radiation with frequency-energy characteristics and a spectral generation range that allows remote determination of background concentrations of greenhouse gases in the atmosphere. The aim of this work was to create a frequency parametric converter based on ZGP, pumped by Ho:YAG laser radiation. For use as a source in a mobile lidar for remote determination of the concentration of greenhouse gases in the atmosphere. In the course of the research, a layout of an Optical parametric oscillator OPO based on a ZGP crystal with Ho:YAG laser radiation pumping was developed. The system's continuous failure-free operation time was 1.5 h at a pulse repetition rate of 10 kHz and a pulse energy of the generated radiation of 0.08 mJ. The tuning range of the OPO was from 3.3 to 5 μm when using a Lyot filter. The losses from the average generation power when the Lyot filter was introduced into the resonator were 30%. At the same time, it was possible to achieve a linewidth of the generated radiation of 0.7 nm. The divergence of the generated radiation did not exceed 1.5 mrad.The absorption spectrum of gases CO_2, CH_4, N_2O, CO in a gas cell was simulated for the entire generation range of the ZnGeP2-based OPO. As a result of the simulation, the most intense absorption lines of gases CO_2, CH_4, N_2O, CO in the OPO tuning range were revealed, the central wavelengths of the absorption lines and their spectral width were determined.

KEYWORDS

ZnGeP2 single crystal, optical parametric oscillator, remote gas analysis, laser-induced damage threshold, greenhouse effect

1 Introduction

The problem of mitigating the effects of climate change caused by the greenhouse effect is becoming one of the defining factors of both foreign and domestic policy in most countries in the world. The main contribution to climate change is made by emissions of such greenhouse gases as: carbon dioxide (CO_2), methane (CH_4), and nitrous oxide (N_2O). Among the instruments aimed at limiting and reducing greenhouse gas emissions, the most flexible and effective are considered to be economic (market) instruments, that is, those that create a *de facto* "carbon price." The most popular of such instruments are carbon taxes and

emissions trading systems (ETS). In the near future, the share of global emissions covered by quotas will increase. These instruments for stimulating the reduction of greenhouse gas emissions are enshrined in the UN Framework Convention on Climate Change, the Kyoto Protocol and the Paris Agreement.

The above circumstances require the creation of an effective technological base for the production of instruments for continuous monitoring of the distribution and dynamics of the concentration of background greenhouse gas components to observe the increase in the total content of these gas components over large areas with the possibility of determining the contribution to the emission of each specific industrial enterprise. The use of spectroscopic probing methods for solving the problem of greenhouse gas emission control, in contrast to standard gas analysis methods, has several undoubted advantages in the rapid non-contact acquisition of the necessary data for studying the composition and physical parameters of the atmosphere. Laser locators (lidars) allow confident detection of local gas formations, plumes of industrial emissions, and the identification of increased content of organic and other hazardous impurities, which pose a potential threat of an environmental catastrophe. The infrared (IR) spectral range is of considerable interest in terms of detecting increased levels of greenhouse and technogenic gases in the atmosphere, since it is in this range that the vibrational-rotational spectra of the main atmospheric pollutants have specific features, which facilitates their identification. In particular, the vibrational-rotational spectra of greenhouse gas components have fairly intense absorption lines in the wavelength range from 1.5 to 5 μm, corresponding to the near and mid-IR region of the optical spectrum. In this regard, the need for developing an IR laser-location system in this wavelength range for solving the problems of sounding one or several gases is greatly increasing.

There are several methods for studying and detecting atmospheric gases, among which a special place is occupied by the method of remote detection and identification of gas traces using selective absorption of laser radiation, which has maximum sensitivity when probing gas components over long distances (differential absorption method or DIAL) [1–4]. The main problem with the practical implementation of DIAL—Differential Absorption Lidar today is the lack of highly monochromatic laser sources of sufficient power in the near and mid-IR ranges, which allow smooth and/or discrete frequency tuning of the radiation. Modern sources of laser radiation for solving atmospheric problems are created based on wide-range IR molecular lasers, as well as parametric frequency converters based on nonlinear crystals, which allow, by generating overtones, harmonics, sum and difference frequencies of laser radiation, to cover the spectral range from 2 to 18 μm. The development of this range, as the most promising for controlling almost all gas components of the atmosphere by the differential absorption method, is currently an urgent task, since the radiation spectra of existing lasers with energy parameters acceptable for use in remote sensing cover only some parts of the specified range. One of the possibilities for obtaining tunable laser radiation in these ranges is to use tunable sources of coherent radiation based on optical parametric oscillator (OPO) using nonlinear crystals. Important parameters of OPO for implementation in remote sensing are low angular divergence of radiation, narrow spectral width, and high output radiation energy. Advances in the research and production of optical crystals allow the development of more and more new gas analysis systems, implemented in the works [5–16], and thereby expand the possibilities of remote monitoring of the environmental state. Let us consider the currently relevant issue of laser remote monitoring of CH4. There are four main absorption bands of methane: near 1.65 μm, 2.3 μm, 3.3–3.4 μm, and 7.7 μm [17]. The most commonly used for laser remote sensing of methane are the methane absorption bands near 1.65 and 3.3 μm, and the sensing technologies in these wavelength ranges are the most developed. The systems discussed in [18–21] operate at λ = 1.65 μm, while those in [22, 23] operate at λ = 3.3–3.4 μm.

The authors of the work [17] found that the productivity of any DIAL system depends on the observation scenario. In general, systems at wavelengths near 3.3 μm can detect smaller methane leaks with higher precision than in the 1.65 μm region.

Accordingly, it is preferable to use absorption lines lying in the three-micron region and falling within the atmospheric transparency window to create a radiation source for a lidar. The acceptable probing height for airborne lidar systems is determined by the safe flight altitude of the aircraft on which the system is mounted and is between 50 and 600 m. Nowadays, lidar complexes have been created to determine the natural gas leaks with an operating wavelength of 3.3922 μm (methane absorption line) and an auxiliary 3.3919 [24] based on commercially produced He-Ne lasers. The disadvantages of these devices include the low average power of the radiation source ~20 mW, providing a probing height of 40–60 m. Lidars based on chemical, CO-, and CO_2-lasers are also known [25, 26]. The disadvantages of these lasers are the need for periodic reloading of the working mixture and large dimensions. In many countries, attempts are being made to create powerful semiconductor lasers operating in the mid-IR range [27]. However, at present, the energy characteristics of such lasers in the wavelength range ~2–4 μm are rather low (average power ~100 mW), which prevents their use in remote methane concentration determination. For this reason, the development of a compact source with energy and spectral characteristics that allow for monitoring greenhouse gas emissions at heights of ~ several hundred metres is a relevant task. One of the possible ways to solve this problem is to develop a source based on the principle of OPO in nonlinear crystals.

For effective operation of the OPO, it is necessary to use crystals with high optical transparency in the given wavelength range, a large value of quadratic nonlinear susceptibility, a high optical breakdown threshold, and good spatial homogeneity. Some of the popular nonlinear materials suitable for generating radiation in the wavelength range of 2–5 μm using OPO are ferroelectric oxides such as lithium niobate ($LiNbO_3$), potassium titanyl phosphate (KTP), potassium titanyl arsenate (KTA), and rubidium titanyl arsenate (RTA). OPO in such structures is achieved through quasi-phase matching, obtained due to the periodically polarized structure of these materials. This, in particular, allows the use of the largest nonlinear optical tensor element d33 for nonlinear conversion, however, the nonlinearity of these materials is still lower than that of ternary compounds with a chalcopyrite crystal lattice type [28].

The most popular materials for OPOs in the wavelength range of 3–12 μm are nonlinear crystals based on ternary compounds: $AgGaS_2$, $AgGaSe_2$, $ZnGeP_2$, and $BaGa_4Se_7$. In [29] was obtained OPO in the wavelength range of 3.26–5.34 μm with a pulse energy of the generated radiation of 0.65 μJ, a repetition rate of 50 Hz, and a conversion efficiency of ~10% when pumping a LiNbO3 crystal with laser radiation from a Tm:YAG laser at 2.01 μm. In [30], OPO was obtained in the wavelength range of 1.8–2.39 μm at a pulse repetition rate of 20 Hz and an efficiency of ~50% with a pulse energy of 1.8 μJ when pumping a KTP crystal with an Nd:YAG laser. In [31], OPO in KTA was implemented with pumping at a wavelength of 1.064 μm. OPO in the wavelength range of 3.47 μm was obtained in the idle channel with an average power of the generated radiation of ~500 mW with a nanosecond pulse duration. In [32], OPO was obtained in the wavelength range of 3.9–11.3 μm with a pulse energy of ~0.37 μJ/cm2 and a conversion efficiency of 22% on an AGS nonlinear crystal when pumped with radiation at ~1 μm. OPO was also obtained in an $AgGaSe_2$ single crystal in the wavelength range of 2.65–9.05 μm with a conversion efficiency of ~18% when pumped with radiation at 2.05 μm [33]. It should be noted that the low thermal conductivity and low optical breakdown threshold ~0.25 J/cm^2 of AGS and $AgGaSe_2$ single crystals limit their use as nonlinear elements for OPO of mid-IR radiation. In [34], an OPO based on a $BaGa_4Se_7$ crystal was implemented with pumping by pulsed radiation at a wavelength of 1.064 μm. The spectral range of the generated radiation was from 3.42–4.73 μm for the idle wave. The average power of the output radiation was 250 mW at a pulse repetition rate of 250 Hz. Notably, the low thermal conductivity of these crystals limits the repetition rate of OPOs developed on their basis, which is limited to a repetition rate of ~200 Hz.

Among all the characteristics, the $ZnGeP_2$ single crystal is one of the most effective for OPO in the wavelength range of 3–5 μm (out of a wide variety of nonlinear optical crystals) [28].

The $ZnGeP_2$ single crystal has an absorption coefficient of <0.02 cm^{-1} in the spectral range of 2.05–8.3 μm [28]. The most powerful OPOs in the 3.3–5.5 μm wavelength range are based on $ZnGeP_2$ (ZGP) single crystals [35]. ZGP-based OPOs generate radiation with an average power of up to 200 W and/or pulse energy of up to 200 mJ at pulse durations of 20–40 ns and repetition rates from a few hertz to hundreds of kilohertz [36–38]. However, the failure-free operation time of these OPOs under the above extreme pumping conditions has to be deliberately limited to a few seconds to avoid optical breakdown of the crystal surface caused by accumulation effects. These sources must be able to operate continuously for several hours at a time, and the total system failure-free operating time must be more than 1,000 h.

It is also worth noting that remote gas analysis requires laser systems with a spectral width of the generated radiation of ≤1 nm. As far as the authors are aware, despite all the advantages of the frequency-energy characteristics of ZGP-based OPOs over other sources of radiation in the 3–5 μm wavelength range, narrow-band generators in the 3–5 μm spectral range have not been created based on ZGP. Since ZGP-based OPOs without introducing selective elements into the resonator have a spectral width of the generated radiation in the range of several hundred nanometers, which does not allow these systems to be used directly for atmospheric sounding.

This work aims to develop and create a radiation source for a remote airborne lidar based on a ZnGeP2 crystal-based optical parametric frequency converter pumped by a Ho:YAG laser for remote monitoring of greenhouse gas emissions in the atmosphere. This will allow the outstanding frequency-energy characteristics of ZGP-based OPOs to be used to solve remote sensing tasks.

2 Development and creation of a optical parametric oscillator layout based on a ZnGeP2 crystal

To create a OPO based on a ZnGeP2 crystal, a nonlinear ZGP crystal (manufactured by LLC "LOK," Tomsk) with linear dimensions of 20 × 6 × 6 mm was fabricated, cut at angles θ = 54.5° and φ = 0°, with antireflection coatings applied to the working, ends at wavelengths λ = 2.097 μm and λ = 3–5 μm. The absorption of radiation at a wavelength of 2.097 μm of the sample was 0.025 cm–1.

A two-stage Lyot filter was used in the layout, located in the resonator of the OPO between the dichroic output mirror and the blind mirror. The Lyot filter was formed by a pair of birefringent plane-parallel plates with an aperture diameter of 30 mm, made of ZGP, cut parallel to the optical axis (100), with thicknesses d1 = 2 mm and d2 = 6 mm. The plates were placed in a frame fixed on a rotary table. The frequency tuning of the generation was carried out by rotating the frame with the plates around the normal to their faces.

In a multi-component Lyot filter (consisting of N elementary Lyot filters), its free dispersion region is determined by the thickness of the thickest filter plate as shown in Eq. 1 [39].

$$\delta\nu = c[(n_o - n_e)L]^{-1} \tag{1}$$

Where c—speed of light, L—the thickness of the plate, n_o, n_e—the refractive indices for the ordinary and extraordinary waves, respectively.

The transmittance T(λ) of a single-stage Lyot filter is given by Eq. 2

$$T(\lambda) = \frac{I_{\text{Цр}}}{I_0} = T_0 \cos^2\left(\pi \frac{\Delta n L}{\lambda}\right) \tag{2}$$

For a multi-stage Lyot filter consisting of plates with different thicknesses Lm, the total transmittance $T(\lambda)$ will be equal to the sum of the individual transmittances Tm(λ) by Eq. 3.

$$T(\lambda) = \sum_{m=1}^{N} T_{0m} \cos^2\left(\pi \frac{\Delta n L_m}{\lambda}\right) \tag{3}$$

Thicknesses L_m of the plates in a multi-stage Lyot filter are chosen to be multiples of a certain value. Rotating the plates of the Lyot filter around an axis perpendicular to the filter surface leads to a shift in the wavelength of the laser radiation. Based on the presented expressions, the Lyot filter used in this work allowed for the

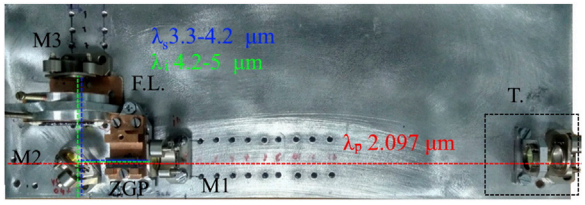

FIGURE 1
Photograph of the resonator of the OPO. T, Telescope formed by two lenses; M1, resonator mirror; ZGP, nonlinear element; M2, dichroic mirror; F.L., interference-polarization filter; M3, blind mirror; λ_p, λ_s, λ_i., pump, signal and idler wavelengths, respectively.

guaranteed generation of a single OPO generation peak without parasitic maxima with a linewidth of ~1 nm.

A pulsed-periodic laser based on Ho:YAG crystals pumped by a thulium fiber laser was used as a pump source for the OPO based on a ZGP single crystal. The Ho:YAG laser had the following energy characteristics: maximum average output power in pulsed mode—15 W, pulse repetition rate—10 kHz, pulse duration at half height—26 ns. The wavelength of the radiation generated by the Ho:YAG laser was 2.097 μm. The amplitude, duration, and energy of the nanosecond pulses of the Ho:YAG laser, as well as the beam diameter, were stable under constant pumping (random fluctuations in the pulse amplitude did not exceed 5%) [40]. The total number of pulses was determined by their repetition rate and exposure time. For each individual series of measurements at the same repetition rate, the number of pulses during the exposure time remained unchanged. To avoid changes in the pulse duration and shape of the generated beam of the Ho:YAG laser, the average power of the pump radiation from the thulium fiber laser was kept the same in all experiments and was equal to ~30 W. The maximum average power of the radiation generated by the Ho:YAG laser was 15 W in a linearly polarized high-quality Gaussian beam (M2 parameter = 1.2). The L-shaped OPO resonator was formed by a mirror M1 with a radius of curvature R- 300 mm with a transmission of ~99% at the pump wavelength and a reflection of ~99% at the generated wavelength. The dichroic plane-parallel mirror M2 with a transmission of ~99% at the pump wavelength and a transmission of 50% at the generation wavelength was placed at an angle of 450 relative to the incident radiation. The blind mirror M3 had a gold coating. This resonator scheme allowed for single-pass pumping. A ZGP single crystal was placed in the resonator. The Lyot filter ¬– F.L. was placed in the part of the resonator where there was no pump radiation, which significantly reduced the optical and thermal load on this selective element, which allowed achieving stable operation of the filter without the use of cooling systems. Figure 1 shows a photo of the resonator of the OPO, and its diagram in Figure 2.

The generated radiation spectrum was measured using an MDR-21 monochromatic (input and output slit width—100 μm, with a diffraction grating of 150 lines/mm and a Hamamatsu photodiode operating in the range of 2.5–4.2 μm.

Figures 3, 4 show the results obtained when measuring the energy characteristics of the OPO layout with a Lyot filter introduced into the resonator (curves –1 Figures 3A, B) and without it, the scheme of which is shown in Figure 2.

The maximum value of the generation efficiency achieved in the experiment with the Lyot filter introduced into the resonator was 28%. The maximum value of the average power of the generated OPO radiation was 1.6 W at a pulse repetition rate of 10 kHz and with the Lyot filter introduced into the resonator. Measurements carried out with a filter that cuts off the idle radiation showed that there is a uniform distribution of intensity between the signal and idle waves.

Figure 4 shows the spectrum of the signal wave of the generated radiation with the Lyot filter removed from the resonator, the spectral width is ~250 nm. The spectrum of the generated radiation with the Lyot filter introduced into the resonator is shown in Figure 8. The width of the generated line at half height was 0.7 nm. The losses from the average generation power when the Lyot filter was introduced into the resonator were 30%.

Figure 5 demonstrates the possibility of tuning narrowband radiation by adjusting the Lyot Filter within the range of signal

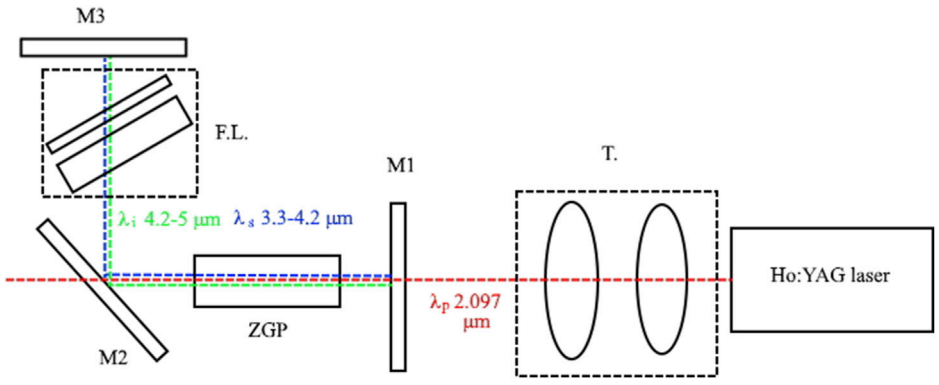

FIGURE 2
Scheme of the setup: T, Telescope formed by two lenses; M1, resonator mirror; ZGP, nonlinear element; M2, dichroic mirror; F.L., interference-polarization filter; M3, blind mirror; λ_p, λ_s, λ_i., pump, signal and idler wavelengths, respectively.

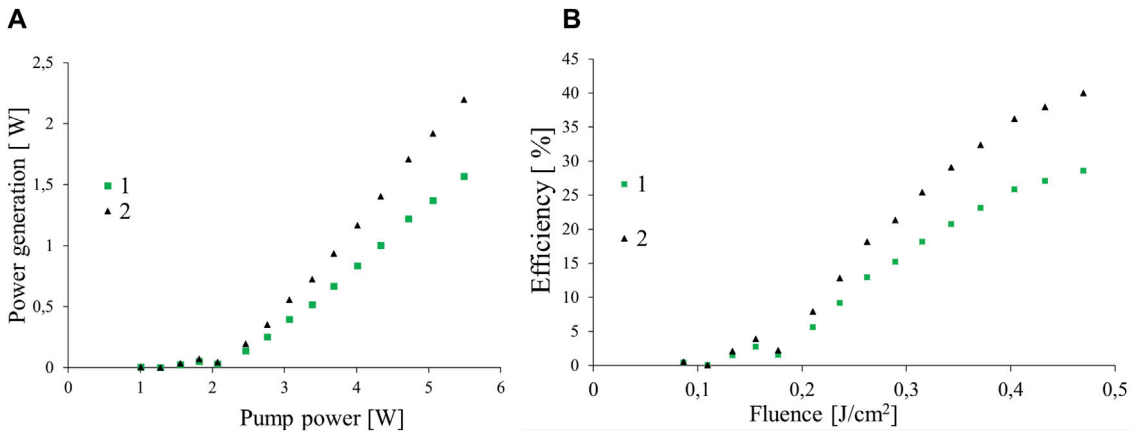

FIGURE 3
(A) Dependence of the OPO generation power on the pump radiation power; **(B)** Efficiency of the generated radiation on the pump radiation energy density. Curves 1—energy parameters of generation with a Lyot filter introduced into the resonator, curves 2—energy parameters of generation in the absence of Lyot filters in the OPO resonator.

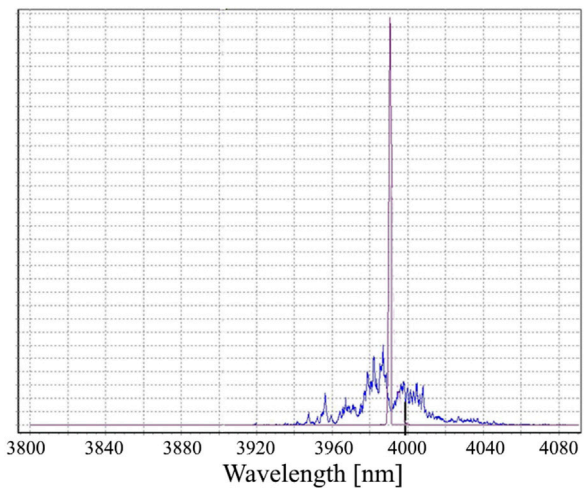

FIGURE 4
Violet curve—spectrum of the generated radiation when the Lyot filter is introduced into the resonator, blue curve—spectrum of the generated radiation when the Lyot filter is removed from the resonator.

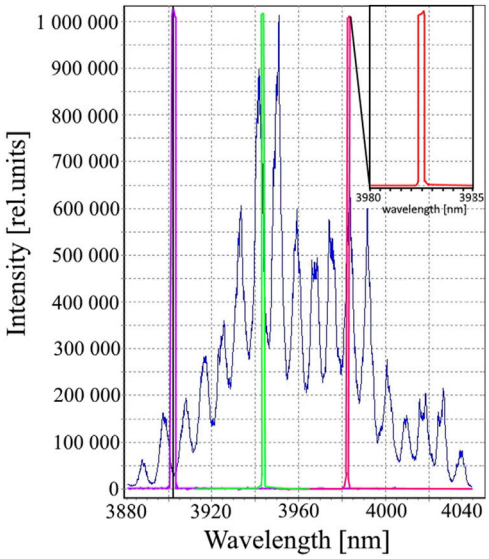

FIGURE 5
Dependence of the intensity of the generated OPO radiation on the wavelength obtained using the MDR-23 monochromator. Blue curve—without the Lyot Filter inserted into the resonator, violet curve, green curve, red curve—generation lines with the Lyot Filter inserted into the OPO resonator at different positions of the filter plates.

wave generation while maintaining a constant angle θ between the axis C of the ZGP crystal and the direction of incidence of the Ho:YAG laser pump radiation. Figure 5 also includes an enlarged inset to demonstrate the linewidth of the generated OPO lines with the Lyot filter inserted into the resonator. As can be seen from the inset in Figure 5, the linewidth of the generated lines is 0.7 nm at the base.

Tuning of narrowband radiation within the spectral range of 3.3–5 μm was carried out by changing the rotation angle of the ZGP crystal (the angle θ between the axis C of the crystal and the direction of incidence of the pump radiation) and adjusting the Lyot filter. Information on the angles θ and wavelengths of the generated OPO radiation is presented in Figure 6. Figure 6 also shows the calculated tuning curve as a function of the change in angle θ, calculated using the SNLO software package.

The discrepancies between the theoretical values of the synchronization conditions and the experimentally obtained values can be explained by inaccuracies in determining the angle between the direction of incidence of the pump radiation and the axis of the ZGP crystal C. Also, the discrepancies may be due to differences in the refractive index values of the ZGP crystals used in the experiment from the

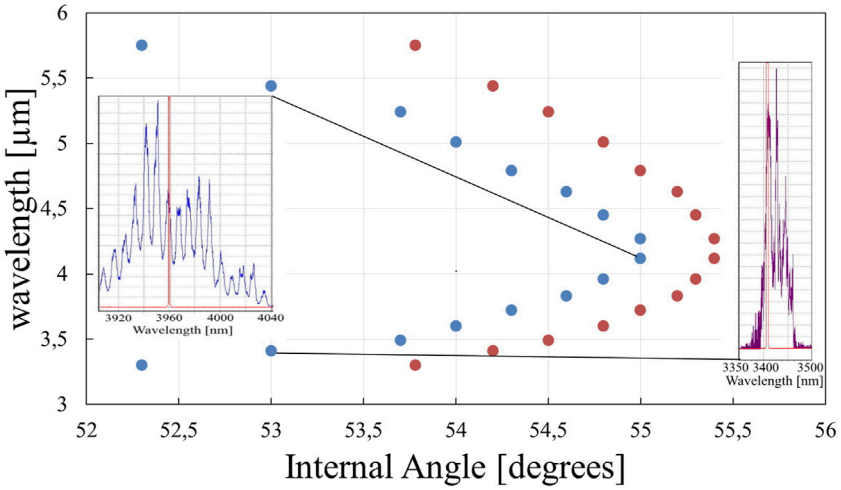

FIGURE 6
Dependence of the wavelength of the generated OPO radiation on the angle θ. Blue dots—experimentally obtained values, insets show experimental spectra of the generated OPO radiation without the Lyot Filter and with the filter inserted into the resonator, red dots—theoretical values obtained using the SNLO software product.

FIGURE 7
Photograph of the housing of the layout of the Optical parametric oscillator based on the ZnGeP2 crystal with intra-resonator radiation selection.

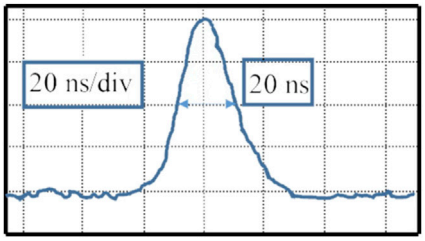

FIGURE 8
Oscillogram of the duration of the radiation pulses generated by the OPO.

tabular values used in SNLO to calculate the phase-matching conditions.

The tuning range of the narrow-band radiation in the region of the signal and idle waves was from 3.3 to 5 μm depending on the rotation angle of the crystal, while the pulse energy of the radiation in the entire tuning range was not less than 0.08 mJ. In the wavelength range of 3.5–5 μm, the pulse energy of the radiation was not less than 0.15 mJ. The divergence of the generated radiation did not exceed 1.5 mrad.

A housing for the OPO layout based on a ZnGeP2 crystal was developed, which is shown in Figure 7.

Pulse duration measurements of the OPO output in the 3.3–5 μm wavelength range were also performed. The results are presented in Figure 8.

Measurements of the beam intensity distribution across the diameter (Figure 9), OPO beam divergence, and pump radiation divergence were performed according to the method described in [41], using a PIROCAM III camera and an interference filter that reflected ~99% of the pump radiation and transmitted ~40–60% of the PG radiation. Initially, the diameter of the radiation—d_1 was measured in the transverse cross-section of the far-field beam, then the Pirocam III was moved away to a distance—L and the diameter of the PG radiation - d_2 was measured again. The divergence angle was calculated using Eq. 4:

$$\theta = \mathrm{arctg}(d_2 - d_1)/L \quad (4)$$

The divergence angle of the pump radiation was ~1.2 mrad. The divergence angle of the PG radiation was 1.5 mrad on the X-axis and 1.6 mrad on the Y-axis. The $M^2_{X,Y}$ parameter for the pump radiation beam was 1.2, and for the PG radiation, the M^2_X parameter was ~2.8 and the M^2_Y parameter was ~2.5.

Power fluctuations of the ZGP OPO radiation were 7% (root mean square) when the OPO was operated for 1.5 h at maximum output power. The output power of the Ho:YAG laser was more stable with power fluctuations of 5% (root mean square), as shown in Figure 10.

Power fluctuations of the ZGP OPO radiation and power fluctuations of the Ho:YAG laser are caused by the instability of the pumping diodes of the Tm:YLF laser, which pumps the Ho:YAG laser.

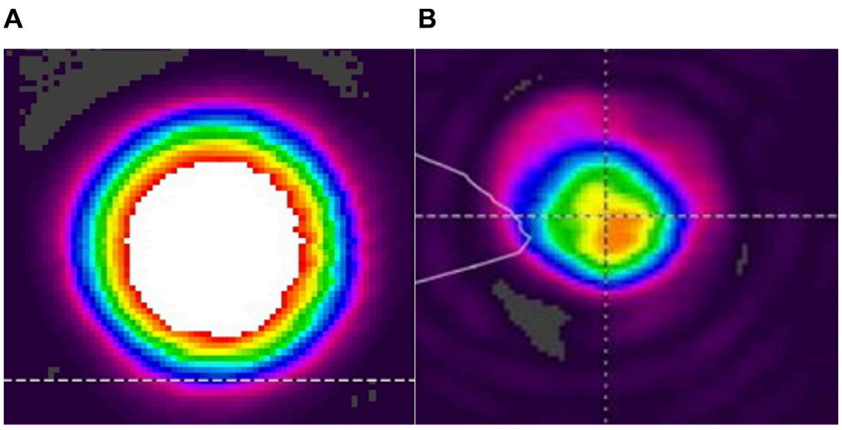

FIGURE 9
(A) Intensity distribution of the pump radiation, **(B)** Intensity distribution of the generated OPO radiation.

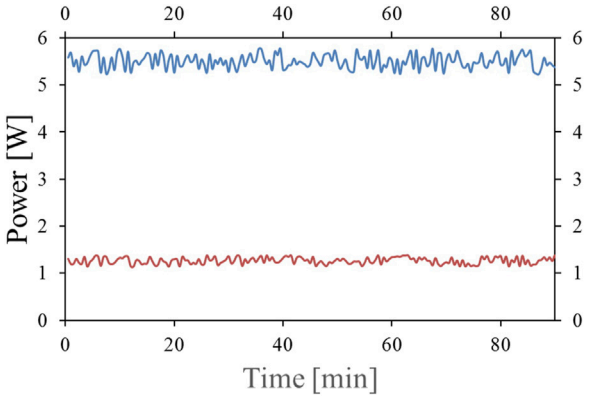

FIGURE 10
Stability of the output power of the Ho:YAG pump laser—blue line and OPO—red line at maximum power for 90 min of operation.

Phase noise is a critical performance parameter for both optoelectronic oscillators [42–44] and OPOs [45, 46].

It should be noted that an open resonator consisting of flat-spherical mirrors (total resonator length L = 101 mm) was used as the resonator of the OPO in this work. Based on Figures 9A, B, the intensity distribution of the pump radiation in the laser beam cross-section had a Gaussian shape, and the radiation generated by the OPO also had an intensity distribution close to Gaussian in the beam cross-section. This indicates that TEM00q longitudinal modes propagate in the OPO resonator. Based on the results presented in [45, 46], under these conditions, the main factor causing phase noise in the OPO is the variation of the resonator's optical length due to mirror vibrations and thermal expansion of the nonlinear crystal due to the absorption of pump laser radiation. The parameters of the OPO presented in this work and in [45] are practically fully comparable. At the same time, the estimates presented in [45] show that under these pumping conditions and OPO parameters, the real fluctuations of the resonator length caused by the reasons mentioned earlier are ~100 nm. The calculations and experimental data presented in [45] show that the average value of the phase noise power per longitudinal mode of the signal and idler waves of the OPO is $4{\cdot}10^{-10}$ W. In the approximation of equidistance of the longitudinal modes of the OPO resonator, based on the fact that the OPO resonator is flat-spherical, the distance between two neighboring longitudinal modes of the resonator is calculated according to the following expression (Eq. 5):

$$\Delta\nu = \frac{c}{2L} \tag{5}$$

where $\Delta\nu$- spacing between two neighboring longitudinal modes, c—light speed, L-resonator length.

Based on expression (4), the spacing between two neighboring longitudinal modes for the OPO resonator presented in this work is 1.485 GHz. In this case, the spectral linewidth of the generated OPO radiation with a $LiIO_3$ filter inserted into the resonator is ~30 GHz (~1 nm). Consequently, ~20 longitudinal modes are formed in the OPO resonator considered in this work.

Thus, based on the presented estimates and results in [45], the maximum phase noise power within the OPO generation spectrum is $\sim 8{\cdot}10^{-9}$ W.

Based on the results presented in Figure 10, it is evident that the power fluctuations of the generated OPO radiation caused by the instability of the Tm:YLF laser pumping diodes, which pumps the Ho:YAG laser, are $\sim 1{\cdot}10^{-1}$ W and are eight orders of magnitude higher than the contribution to the power fluctuations of the generated radiation caused by phase noise. Thus, this allows us to neglect the contributions of this effect to the stability of the OPO operation under the pumping conditions presented in this work.

Thus, in the course of the research, it was possible to create a layout of an OPO based on a ZGP crystal that generates radiation with a spectral width of 0.7 nm and a pulse energy of 0.08 mJ at a pulse repetition rate of 10 kHz and a pulse duration of 20 ns. The tuning range was from 3.3 to 5 μm. The continuous operation time of the system was 1.5 h. The divergence of the generated radiation did not exceed 1.25 mrad.

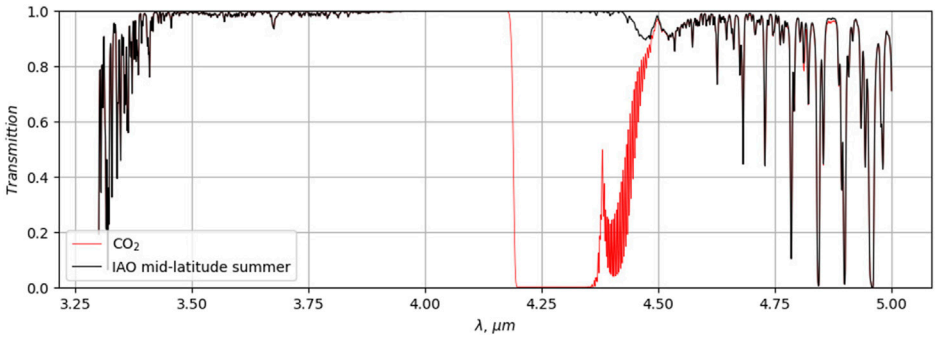

FIGURE 11
Transmission spectrum of the atmosphere in the wavelength range of tuning of the developed OPO based on the ZGP crystal for CO_2 (path length 100 m).

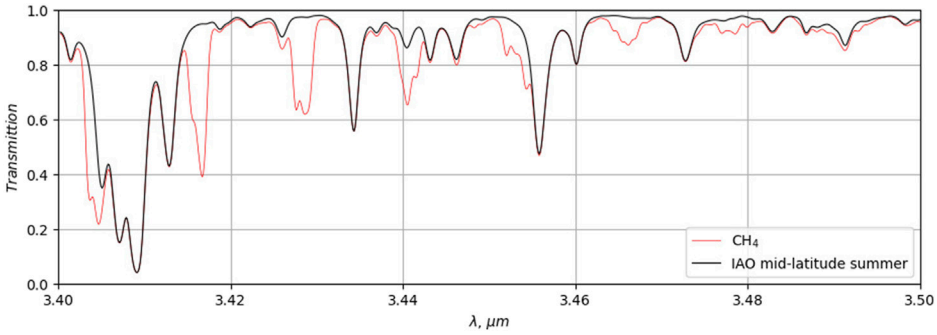

FIGURE 12
Transmission spectrum of the atmosphere in the wavelength range of tuning of the developed OPO based on the ZGP crystal for CH_4 (path length 1,000 m).

3 Modeling of CO_2, CH_4, N_2O, CO absorption spectra in a gas cell for the generation range of a $ZnGeP_2$-Based OPO with different radiation linewidths

Modeling of the transmission spectra of CO_2, CH_4, N_2O, and CO in the tuning range of the developed ZGP-based OPO 3.3–5 μm (2000–3,030 cm−1) was performed using the SPECTRA software [47] and the HITRAN spectroscopic database [48]. The modeling of the spectra is based on the method of poly-linear calculation of the spectral absorption contour of substances in the gas phase, which is a summation of the standard absorption contours of isolated lines. As a rule, the lines represent vibrational-rotational transitions grouped into separate vibrational bands. The positions of the line centers and their intensities are recorded under certain conditions with high-resolution spectrometers. When modeling the spectra, the data selection is carried out in the section molecule/isotope/spectral bands or a given frequency range for the selected molecule or for the selected or user-defined gas mixture.

As a result of the modeling, the transmission spectra of the atmosphere in the background conditions of mid-latitude summer were obtained for the wavelength range of the developed ZGP-based OPO. The analysis was carried out for CO_2, CH_4, N_2O, and CO gases at a temperature of 292 C, a pressure of 1 atm, at different optical path lengths, and a laser generation line width of 0.7 nm. The results are presented in Figures 6–9. The black curves in Figures 11–14 represent the atmospheric transmission spectra under background summer conditions in mid-latitudes for the wavelength range of the ZGP-based OPO, and the red curves represent the transmission spectra for selected gases at a temperature of 292 C and a pressure of 1 atm. Accordingly, the results presented in Figures 11–14 show informative absorption lines of selected gases lying in the region of atmospheric transparency, which will allow them to be used for remote sensing of background concentrations of these greenhouse gases.

From the results presented in Figures 11–14, it is seen that for each of the generation sub-ranges, with different lengths of the sounding path, it is possible to conduct a study of the background concentration of the target gas in the atmospheric transparency windows (Table 1).

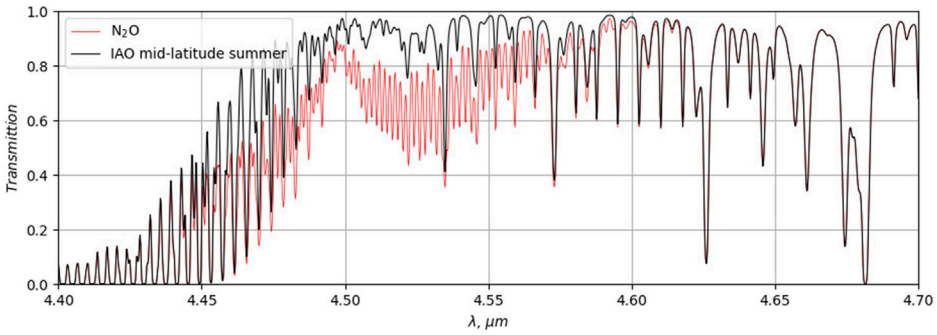

FIGURE 13
Transmission spectrum of the atmosphere in the wavelength range of tuning of the developed OPO based on the ZGP crystal for N_2O (path length 500 m).

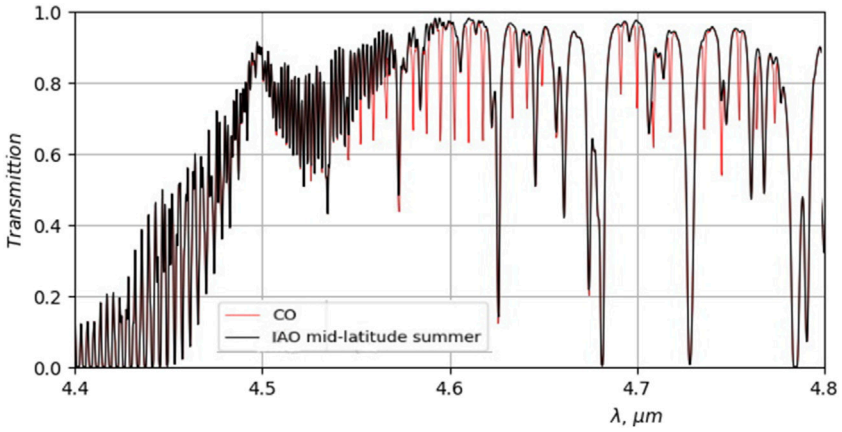

FIGURE 14
Transmission spectrum of the atmosphere in the wavelength range of tuning of the developed OPO based on the ZGP crystal for CO (path length 400 m).

TABLE 1 Information on absorption lines for gases CO2, CH4, NO2, CO in the tuning range of the OPO, central wavelengths of absorption lines, absorption line widths.

Gas	Spectral line width, nm	Central absorption line wavelength, μm	Maximum length of sounding path, m
CO_2	125	4.375	100
CH_4	4	3.4048	1,000
CH_4	2	3.418	1,000
CH_4	4	3.4288	1,000
CH_4	4	3.445	1,000
N_2O	50	4.525	500
CO	0.25	4.587	400
CO	0.25	4.612	400

4 Conclusion

In this work, a layout of a OPO based on a ZGP crystal pumped by Ho:YAG laser radiation was developed. The continuous operation time of the system without failure was 1.5 h at a pulse repetition rate of 10 kHz and a pulse energy of the generated radiation of 0.08 mJ. The tuning range of the OPO was from 3.3 to 5 μm when using a Lyot filter. When tuning the radiation generated in the OPO in the wavelength range of 3.5–5 μm, the pulse energy of the radiation was 0.15 mJ. The losses from the average generation power when the Lyot filter was introduced into the resonator were 30%. At the same time, it was possible to achieve a linewidth of the generated radiation of 0.7 nm. The divergence of the generated radiation did not exceed 1.5 mrad. The absorption spectrum of CO_2, CH_4, N_2O, and CO gases in a gas cell was modeled for the entire generation range of the $ZnGeP_2$-based OPO. As a result of the modeling, the most intense absorption lines of CO_2, CH_4, N_2O, and CO gases in the OPO tuning range were identified, and the central wavelengths of the absorption lines and their spectral width were determined.

Data availability statement

The original contributions presented in the study are included in the article/Supplementary material, further inquiries can be directed to the corresponding author.

Author contributions

NY: Writing–original draft, Writing–review and editing. MZ: Writing–original draft, Writing–review and editing. SP: Writing–original draft, Writing–review and editing. VK: Writing–original draft, Writing–review and editing. ES: Writing–original draft, Writing–review and editing. AL: Writing–original draft, Writing–review and editing. AK: Writing–original draft, Writing–review and editing. AG: Writing–original draft, Writing–review and editing. SY: Writing–original draft, Writing–review and editing. SS: Writing–original draft, Writing–review and editing. OR: Writing–original draft, Writing–review and editing. HB: Writing–original draft, Writing–review and editing.

Funding

The author(s) declare that financial support was received for the research, authorship, and/or publication of this article. The study was supported by the Russian Science Foundation grant No. 23-79-10193, https://rscf.ru/project/23-79-10193/

Conflict of interest

The authors declare that the research was conducted in the absence of any commercial or financial relationships that could be construed as a potential conflict of interest.

Publisher's note

References

1. Collis RTH, Russell PB *Lidar measurement of particles and gases by elastic backscattering and differential absorption*. New York: Springer (1976).

2. Vasil'ev BI, Mannoun UM IR differential-absorption lidars for ecological monitoring of the environment. *Quant Electr* (2006) 36:801–20.

3. Bobrovnikov SM, Matvienko GG, Romanovsky OA, Serikov IB, Sukhanov AY Lidar spectroscopic gas analysis of the atmosphere. *Tomsk: Publishing house IOA SB RAS.* (2014) 510.

4. Nevzorov AA, Nevzorov AV, Penner IE, Romanovsky OA, Samoilova SV, Sukhanov AY, et al. *Lidar monitoring of cloud and aerosol fields, trace gas components and atmospheric meteorological parameters*. Tomsk: Publishing house IOA SB RAS (2015). p. 450.

5. Mitev V, Babichenko S, Bennes J, Borelli R, Dolfi-Bouteyre A, Fiorani L, et al. Mid-IR DIAL for high-resolution mapping of explosive precursors. *Proc SPIE* (2013) 8894: 88940S. doi:10.1117/12.2028374

6. Cadiou E, Mammez D, Dherbecourt J-B, Gorju G, Pelon J, Melkonian J-M, et al. Atmospheric boundary layer CO_2 remote sensing with a direct detection LIDAR instrument based on a widely tunable optical parametric source. *Opt Letters* (2017) 42: 4044–7. doi:10.1364/ol.42.004044

7. Shibata Y, Nagasawa C, Abo M Development of 16 μm DIAL using an OPG/OPA transmitter for measuring atmospheric CO_2 concentration profiles. *Appl Opt* (2017) 56:1194–201. doi:10.1364/ao.56.001194

8. Ayrapetyan VS Measurement of absorption spectra for atmospheric methane by a lidar system with tunable emission wavelength in the range 1.41-4.24 μm. *J Appl Spectrosc* (2009) 76:268–72.

9. Ayrapetyan VS, Fomin PA Laser detection of explosives based on differential absorption and scattering. *Opt Laser Technol* (2018) 106:202–8. doi:10.1016/j.optlastec.2018.04.001

10. Romanovskii OA, Sadovnikov SA, Kharchenko OV, Yakovlev SV Broadband IR lidar for gas analysis of the atmosphere. *J Appl Spectrosc* (2018) 85:457–61. doi:10.1007/s10812-018-0672-y

11. Romanovskii OA, Sadovnikov SA, Kharchenko OV, Yakovlev SV Near/mid-IR OPO lidar system for gas analysis of the atmosphere: simulation and measurement results. *Opt Mem Neural Networks* (2019) 28:1–10. doi:10.3103/s1060992x19010053

12. Romanovskii OA, Sadovnikov SA, Kharchenko OV, Yakovlev SV Development of Near/Mid IR differential absorption OPO lidar system for sensing of atmospheric gases. *Opt Laser Technol* (2019) 116:43–7. doi:10.1016/j.optlastec.2019.03.011

13. Veerabuthiran S, Razdan AK, Jindal MK, Sharma RK, Sagar V Development of 3.0–3.45μm OPO laser based range resolved and hard-target differential absorption lidar for sensing of atmospheric methane. *Opt Laser Technol* (2015) 73:1–5. doi:10.1016/j.optlastec.2015.04.007

14. Mammez D, Cadiou E, Dherbecourt J-P, Raybaut M, Melkonian J-M, Godard A, et al. Multispecies transmitter for DIAL sensing of atmospheric water vapour, methane and carbon dioxide in the 2 μm region. *Proc SPIE* (2015) 9645:964507964507–9.

15. Robinson I, Jack JW, Rae CF, Moncrieff JB Development of a laser for differential absorption lidar measurement of atmospheric carbon dioxide. *Proc SPIE* (2014) 9246: 92460U. doi:10.1117/12.2068023

16. Dawsey M, Numata K, Wu S, Riris H Optical parametric technology for methane measurements. *Proc SPIE* (2015) 9612:961205. doi:10.1117/12.2191615

17. Yerasi A, Tandy WD, Emery WJ, Barton-Grimley RA Comparing the theoretical performances of 1.65- and 3.3-μm differential absorption lidar systems used for airborne remote sensing of natural gas leaks. *J Appl Remote Sens* (2018) 12:1. doi:10.1117/1.jrs.12.026030

18. Bartholomew J, Lyman P, Weimer C. Wide area methane emissions mapping with airborne IPDA lidar. *Procceedings of SPIE* (2017) 10406:1040607. doi:10.1117/12.2276713

19. Frish MB, Wainner RT, Laderer MC, Allen MG, Rutherford J, Wehnert P, et al. Low-cost lightweight airborne laser-based sensors for pipeline leak detection and reporting. *Proc SPIE* (2013) 8726:87260C. doi:10.1117/12.2015813

20. Horn B ALMA provides smarter gas pipeline aerial survey. *Pipeline Gas J* (2014) 241(9):96.

21. Amediek A, Ehret G, Fix A, Wirth M, Budenbender C, Quatrevalet M, et al. CHARM-F—a new airborne integrated-path differential-absorption lidar for carbon dioxide and methane observations: measurement performance and quantification of strong point source emissions. *Appl Opt* (2017) 56:5182–97. doi:10.1364/ao.56.005182

22. Degtiarev EV, Geiger AR, Richmond RD Compact mid-infrared DIAL lidar for ground-based and airborne pipeline monitoring. *Procceedings of SPIE* (2003) 4882: 432–42. doi:10.1117/12.462573

23. Murdock DG Applications of real-world gas detection: airborne natural gas emission lidar (ANGEL) system. *J Appl Remote Sens* (2008) 2:023518. doi:10.1117/1.2937078

24. Andreeva NP, Barashkov MS, Demkin VK, Pechersky EA *Patent "Method for remote detection of environmentally hazardous gases" Pat. 2158423* (2024). Pshenichnikov S.M. No. 99105621/28; application 03/22/1999; publ. 10/27/2000.

25. Koval'chuk LV, Grezev AN, Niz'ev VG, Yakunin VP, Mezhevov VS, Goryachkin DA, et al. Repetitively pulsed TEA CO2 laser and its application for second harmonic generation in ZnGeP2 crystal. *Quan Electron* (2015) 45:884–90.

26. Gaudio P, Malizia A, Gelfusa M, Murari A, Parracino S, Poggi L, et al. Lidar and Dial application for detection and identification: a proposal to improve safety and security. *J Instrumentation* (2017) 12:C01054. doi:10.1088/1748-0221/12/01/c01054

27. Volkov VG Quantum cascade lasers and their applications in security and communications systems. *Control Commun security Syst* (2016) 1:10–41.

28. DmitrievV G, Gurzadyn GG, Nikogosyan DN Handbook of nonlinear optical crystals. *Springer Ser Opt Sci* (1999) 64:407. doi:10.1007/978-3-540-46793-9

29. Xia L, Zhang C The progress of optical parametric oscillator based on $LiNbO_3$ crystal. In: *International symposium on optoelectronic technology and application 2014: infrared technology and applications*. Proc. SPIE 9300 (2014).93000I

30. Hellstrom J, Pasiskevicius V, Laurell F, Karlsson H Efficient nanosecond optical parametric oscillators based on periodically poled KTP emitting in the 18–25-μm spectral region. *Opt Lett* (1999) 24:1233–5. doi:10.1364/ol.24.001233

31. Miao J, Pan Y, Qu S Compact and highly efficient passively Q-switched intracavity KTA-OPO at 1.53 and 3.47 μm. *Chin Phys Lett* (2011) 28:124206. doi:10.1088/0256-307x/28/12/124206

32. Vodopyanov KL, Maffetone JP, Zwieback I, Ruderman W AgGaS2 optical parametric oscillator continuously tunable from 3.9 to 11.3 μm. *Appl Phys Lett* (1999) 75:1204–6.

33. Eckardt RC, Fan YX, Byer RL, Marquardt CL, Storm ME, Esterowitz L Broadly tunable infrared parametric oscillator using AgGaSe2. *Appl Phys Lett* (1986) 49:608–10. doi:10.1063/1.97055

34. He Y, Yan C, Chen K, Xu D, Li J, Zhong K, et al. High repetition rate, tunable mid-infrared Baga4Se7 optical parametric oscillator pumped by a 1 μm Nd:YAG laser. *Appl Sci* (2022) 12:7197. doi:10.3390/app12147197

35. Schunemann PG, Zawilski KT, Pomeranz LA, Creeden DJ, Budni PA. Advances in nonlinear optical crystals for mid-infrared coherent sources. *J Opt Soc Am B* (2016) 33: D36–D43. doi:10.1364/josab.33.000d36

36. Hemming A, Richards J, Davidson AA, Carmody N, Bennetts S, Simakov N, et al. 99 W mid-IR operation of a ZGP OPO at 25% duty cycle. *Opt Express* (2013) 21: 10062–9. doi:10.1364/oe.21.010062

37. Haakestad MW, Fonnum H, Lippert E Mid-infrared source with 02 J pulse energy based on nonlinear conversion of Q-switched pulses in ZnGeP_2. *Opt Express* (2014) 22:8556–64. doi:10.1364/oe.22.008556

38. Qian C, Yao B, Zhao B, Liu G, Duan X, Ju Y, et al. High repetition rate 102 W middle infrared ZnGeP2 master oscillator power amplifier system with thermal lens compensation. *Opt Lett* (2019) 44:715–8. doi:10.1364/ol.44.000715

39. Sinha NK Normalised dispersion of birefringence of quartz and stress optical coefficient of fused silica and plate glass. *Phys Chem Glasses* (1978) 19:69–77.

40. Antipov OL, Kositsyn RI, Eranov ID 36W Q-switched Ho^{3+}: YAG laser at 2097 nm pumped by a Tm fiber laser: evaluationof different Ho3+ doping concentrations. *Laser Phys Lett* (2017) 14:015002. doi:10.1088/1612-202x/14/1/015002

41. Demin VV, Polovtsev IG, Simonova GV *Opticheskie izmereniya (Optical measurements)*. Tomsk: TSU Publishing House (2014). p. 300.

42. Bouchier A, Saleh K, Merrer P-H, Llopis O, Cibiel G Theoretical and experimental study of the phase noise of opto-electronic oscillators based on high quality factor optical resonators. *IEEE Int Frequency Control Symp* (2010) 544–8. doi:10.1109/freq.2010.5556269

43. Tang J, Hao T, Li W, Domenech D, Baños R, Muñoz P, et al. Integrated optoelectronic oscillator. *Opt Express* (2018) 26:12257–65. doi:10.1364/oe.26.012257

44. Brunetti G, Armenise MN, Ciminelli C. Chip-scaled KaBand photonic linearly chirped microwave waveform generator. *Front Phys* (2022) 10:785650. doi:10.3389/fphy.2022.785650

45. Antipov OL, Eranov ID, Kositsyn RI 10-W mid-IR optical parametric oscillators based on ZnGeP2 elements pumped by a fibre-laser-pumped Ho: YAG Laser. *Exp Numer Study Quan Electron.* (2017) 47:601–6.

46. Smith AV, Alford WJ, Raymond TD, Bowers MS. Comparison of a numerical model with measured performance of a seeded, nanosecond KTP optical parametric oscillator. *Opt Soc Am B* (1995) 12(12):2253–67. doi:10.1364/josab.12.002253

47. Mikhailenko SN, Babikov YL, Golovko VF Information and computing system "Spectroscopy of atmospheric gases". Structure and main functions. *Opt atmosphere ocean* (2005) 18:765–76.

48. Gordon IE, Rothman LS, Hill C, Kochanov RV, Tan Y, Bernath PF, et al. *J Quant Spectrosc Radiat Transfer* (2017) 203:3–69.